Journal of Membrane Science & Research

journal homepage: www.msrjournal.com

Research Paper

# Modeling the Effectiveness of Hollow Fiber Membrane Contactors for $CO_2$ Capture Using Ionic Liquids: A Comparative Study

Nayef Ghasem

*Department of Chemical and Petroleum Engineering, United Arab Emirates University, Al-Ain, UAE*

## Article info

Received 2023-06-29
Revised 2023-08-07
Accepted 2023-08-18
Available online 2023-08-18

## Keywords

$CO_2$ capture
Ionic liquids
Hollow fiber membrane
Mass transfer
transient modeling
CFD Simulation

## Highlights

- A comprehensive transient 2D model was developed to predict $CO_2$ capture via three ionic liquids in the membrane contactor.
- The results indicated good agreement between experimental and modeled $CO_2$ removal efficiency.
- The results indicated that emim[$C_2N_2$] gives the best efficiency and the longest lifetime.
- The model evaluated the effect of various input parameters on $CO_2$ capture efficiency.

## Graphical abstract

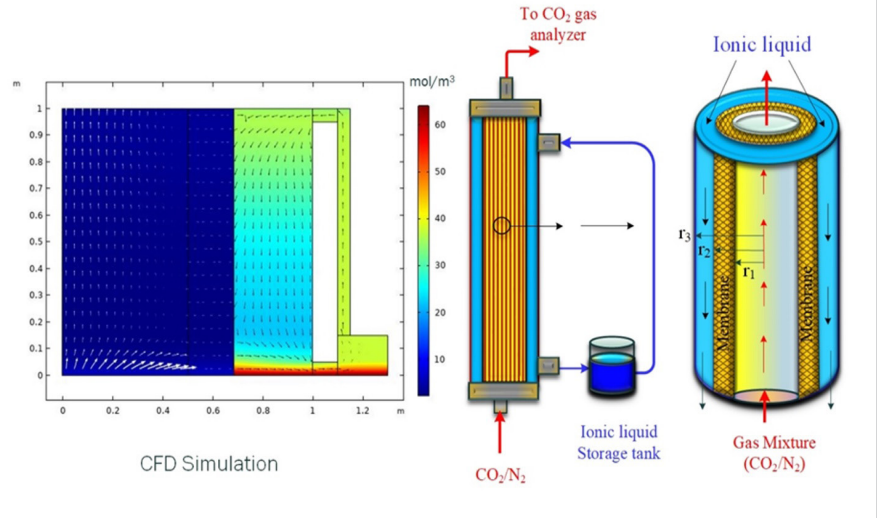


## Abstract

The ability of technology and active solvents to absorb carbon dioxide from natural gas and after-combustion gases and to regenerate used solvents is a key representative of the search for efficient methods and environmentally friendly solvents. This study aims to construct a 2D model to evaluate the effectiveness of a hollow fiber membrane contactor (HFMC), in capturing $CO_2$ using three distinct types of ionic liquids (ILs): 1-butyl-3-methylimidazoliumtriflate (bmim [Triflate]), 1-Ethyl-3-methylimidazolium ethyl sulfate (emim[$EtSO_4$]), and 1-Ethyl-3-methylimidazolium dicyanamide (emim[$C_2N_2$]). The present model considers the storage tank for the solvent and considers its availability over time. By comparing the model predictions with experimental data, the results were in good agreement, with a slight discrepancy in the starting time for $CO_2$ uptake due to a time lag. Among the ILs evaluated, emim [$C_2N_2$] performs the best. Through sensitivity analysis, results reveal that increasing the feed flow rate and $CO_2$ partial pressure enhances both the $CO_2$ removal rate and prolongs solvent life.

### 1. Introduction

Extensive burning of fossil fuels and human activities significantly increases $CO_2$ emissions in the atmosphere and hence contributes to climate change and consecutive global warming. Accordingly, the reduction of these emissions is crucial and requires developing effective $CO_2$ removal strategies. [1,2]. An effective $CO_2$ capture technology is essential before it is released into the atmosphere. By doing this, we can reduce greenhouse gas releases and moderate the negative effects of climate change. The selected $CO_2$ capture technology should be energy-efficient, sustainable, cost-effective, and environmentally friendly [3]. Such technologies are crucial for achieving the goals of global climate and maintaining a sustainable future for our planet. Among these capture technologies are the gas-liquid absorption column and membrane contacting processes [4]. In these technologies the selection of the appropriate solvent is important. The solvent should have a high selectivity for $CO_2$ capture (i.e., can remove a lot of $CO_2$ from the gas stream), be cost-effective, environmentally friendly, and be easy to regenerate (low energy consumption) [5]. Salt solutions of amino acids such as potassium threonate,

* Corresponding author: nayef@uaeu.ac.ae (N. Ghasem)

DOI: 10.22079/JMSR.2023.2005926.1617

potassium lysinate, and potassium sarcosinate were used for reducing $CO_2$ emissions [6].

Ionic liquids (ILs) made of ions instead of molecules are believed to have several advantages over conventional liquid solvents such as alkanolamine solvents. The IL solvent has low volatility (does not evaporate quickly, which prevents the IL from being lost to the atmosphere) and negligible vapor pressure (does not condense easily) that makes them identical to $CO_2$ capture and prevents them from clogging the membrane pores. Amino acids-based ionic liquids (Cholinium lysinate) were found to be effective absorbents for $CO_2$ separation from the gaseous mixture using 2D simulation in a hollow fiber membrane contactor [7]. ILs are stable over a wide range of temperatures, none toxic nor flammable [8–15]. $CO_2$ capture using membrane contactors has emerged as a promising approach to addressing the challenges of reducing greenhouse gas emissions [16]. These innovative devices utilize specialized membranes to selectively separate $CO_2$ from gas streams, offering significant advantages such as high efficiency, low energy consumption, and compact design. The membrane contactor technology facilitates the transfer of $CO_2$ across the membrane, enabling its capture while allowing other gases to pass through. This process not only helps mitigate the environmental impact of $CO_2$ emissions but also presents opportunities for carbon capture and utilization. The application of membrane contactors for $CO_2$ capture represents a valuable strategy in the pursuit of sustainable and eco-friendly solutions to combat climate change. A potential and promising technology for $CO_2$ capture is the hollow fiber membrane contactors (HFMCs) that are composed of a bundle of polymeric or ceramic porous hollow fiber membranes located in a case, arranged like a shell and tube heat exchange. The gas stream flows in the tube side with solvent flows in the shell side or vice versa, in a concurrent or counter-current mode of operation. When the $CO_2$ and solvent come into direct contact, $CO_2$ dissolves in IL liquid which is later generated and used again (Fig. 1). Compared with traditional $CO_2$ capture methods, HFMCs have several advantages such as high selectivity, low energy consumption, high mass transfer rates, and ease of scale-up [17–23].

The use of HFMCs along with ILs is a promising innovative technology that improved the efficiency of $CO_2$ absorption significantly. Several types of ILs exist among those are 1-butyl-3-methylimidazolium trifluoro-methane-sulfonate ([bmim][Triflate]), 1-ethyl-3-methylimidazolium ethyl sulfate ([emim][$EtSO_4$]), and 1-ethyl-3-methylimidazolium dicyanamide ([emim][DCA]), many others are under development and extensive research work is needed to develop ILs that are more cost-effective and environmentally friendly [24–26].

In this study and to the best of the author's knowledge a transient mathematical model was developed for the first time that includes the solvent storage tank and the ionic liquid circulation rate to investigate the potential use of various ILs solvents in HFMCs. Thus, the primary objective is to create a transient 2D mathematical model that can anticipate the point at which the solvents' recirculation becomes inactive and necessitates regeneration. Additionally, a thorough examination of different operating parameters was conducted.

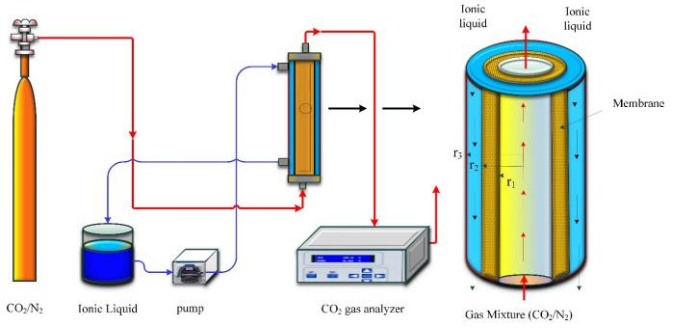


**Fig. 1.** Schematic diagram describes solvent flowing in the membrane shell, while gas mixtures containing 15% $CO_2/N_2$ flow in the membrane shell.

## 2. Model development

Several assumptions were made to develop the mathematical model for $CO_2$ capture using IL systems in HFMCs. The system was assumed to be isothermal. The mass transfer of $CO_2$ between the gas and liquid phases was assumed to be governed by Henry's law and was described using a mass transfer coefficient [27]. The model also accounted for the transport of IL through the HFMCs and the selective membrane coating the fibers. The mass balance equations were developed for the gas and liquid phases, which describe the concentration changes of $CO_2$, IL in the system over time. The equations were solved using numerical methods, and the simulation results were used to evaluate the performance of the IL in HFMCs under various operating conditions. The model development was based on a thorough review of the existing literature on ILs, and HFMCs. The model was validated using experimental data from previous studies, and the simulation results were found to be in good agreement with the experimental data. The overall mass transfer equation will be as follows [28]:

$$\frac{\partial C_i}{\partial t} = D_i \nabla^2 C_i - \nabla . C_i V_z + R_i \tag{1}$$

where $D_i$, is the diffusion coefficient, $V_z$, is the axial velocity along the membrane module length. The reaction rate is $R_i$.

Equation (1) represents the component material balance within the tube ($C_{i,t}$) considering the convective term, diffusion term (with diffusion coefficient $D_{i,t}$), and reaction terms ($R_i$). This is founded upon the assumption of a steady-state condition. The initial point for the convective term is the velocity on the tube side ($V_{z,t}$), while the diffusion term originates from the diffusion coefficient ($D_{i,t}$) [29].

$$D_{i,t}\left(\frac{\partial^2 C_{i,t}}{\partial r^2} + \frac{1}{r}\frac{\partial C_{i,t}}{\partial r} + \frac{\partial^2 C_{i,t}}{\partial z^2}\right) - V_{z,t}\frac{\partial C_{i,t}}{\partial z} + R_{i,t} = \frac{dC_{i,t}}{dt} \tag{2}$$

The velocity profile on the tube side is represented by a parabola using the average velocity ($V_{av}$) and the ratio of the variable radius (r) to the inner radius of the inner tube ($r_1$). This relationship is illustrated by the following equation. The diffusivity in the tube side (gas) can be estimated using the following equation[30].

$$D_{CO_2,g} = \frac{\left(0.01013T^{1.5}\left(\frac{1}{M_{w,CO_2}} + \frac{1}{M_{w,N_2}}\right)\right)}{P\left[(\sum v_{CO_2})^{\frac{1}{3}}(\sum v_{CO_2})^{\frac{1}{3}}\right]} \tag{3}$$

where, T(K) is the temperature, P(Pa) is the pressure, Mw(g/mol) is the molecular weight, and $v$ is the atomic diffusion volume. The Navier-Stocks equation is also applied, revealing notable variations in the velocity profile. The velocity profile inside the hollow fiber ($V_{z,t}$) is described by the parabola [31,32].

$$V_{z,t} = 2v_a\left[1 - \left(\frac{r}{r_1}\right)^2\right] \tag{4}$$

where, $v_a$ is the average velocity, $r_1$ the membrane's inner radius. In the membrane segment, the pores of the membrane are filled with solvents because we assume the wetted mode. Diffusion begins with a parameter called $D_{i,m}$, and the only equations that control the process are related to the reactions taking place. We ignore the convective term. As a result, the concentration profile inside the membrane pores ($C_{i,m}$) reflects the balance of the material components in the following manner [33].

$$D_{i,m}\left(\frac{\partial^2 C_{i,m}}{\partial r^2} + \frac{1}{r}\frac{\partial C_{i,m}}{\partial r} + \frac{\partial^2 C_{i,m}}{\partial z^2}\right) = \frac{dC_{i,m}}{dt} \tag{5}$$

When the solvent is present on the tube side and gas on the shell side, and the membrane is dry (not wetted), the diffusion coefficient of $CO_2$ in the pores of the membrane ( $D_{i,m}$ ) is influenced by three factors: the porosity ($\epsilon$) and tortuosity ($\tau$) of the porous membrane, as well as the diffusion of the component in the shell side ( $D_{i,s}$ ).

$$D_{i,m} = \left[ D_{i,s} \times \frac{\epsilon}{\tau} \right] \tag{6}$$

The distribution pattern of carbon dioxide ( $C_{i,s}$ ) in the outer layer is described by the shell-side diffusion coefficient of $CO_2$ ( $D_{i,s}$ ) and the velocity profile on the outer layer ( $V_{z,s}$ ). There is no chemical reaction happening on this side, except within the falling film [34].

$$D_{i,s}\left( \frac{\partial^2 C_{i,s}}{\partial r^2} + \frac{1}{r}\frac{\partial C_{i,s}}{\partial r} + \frac{\partial^2 C_{i,s}}{\partial z^2} \right) - V_{z,s}\frac{\partial C_{i,s}}{\partial z} = \frac{dC_{i,s}}{dt} \tag{7}$$

The Navier-Stokes equations govern the movement of fluids and can be seen as an extension of Newton's second law of motion specifically designed for liquids. In the case of a compressible Newtonian fluid, the equations yield the following outcomes [29]:

$$\rho\left( \frac{\partial u}{\partial t} + u.\nabla u \right) = -\nabla p + \nabla.\left( \mu\left( \nabla u + (\nabla u)^T \right) - \frac{2}{3}\mu(\nabla.u)I \right) + F \tag{8}$$

where "u" represents the velocity of the fluid, "p" represents the pressure of the fluid, "ρ" represents the density of the fluid, and "μ" represents the fluid's dynamic viscosity.

The diffusivity of $CO_2$ in ionic liquid ( $D_{CO_2,il}$ ) is influenced by the solvent viscosity ( $\mu$ ) and $CO_2$ molar volume ( $v_{CO_2}$ )[35].

$$D_{CO_2,il}\,(cm^2.s^{-1}) = 2.66\times10^3\,\mu^{-0.66}\,v_{CO_2}^{-1.04} \tag{9}$$

The individual terms correspond to the forces exerted on the fluid, including inertial, pressure, viscous, and external forces. Model development utilizes the parameters listed in Table 1. The comparison of the physical properties of the three solvents is listed in Table 2.

Table 3 presents the physical and chemical characteristics employed in the modeling process.

**Table 1**
Ceramic membrane speciation and feed conditions [36].

| Parameters | value |
|---|---|
| Module length (cm) | 11.5 |
| Hollow fiber inner radius (mm) | 0.11 |
| Hollow fiber outer radius (mm) | 0.15 |
| Membrane pore diameter (um) | 0.04 |
| Module packing factor | 0.39 |
| Porosity | 0.4 |
| Inlet concentration of $CO_2$ (vol%) | 15 |
| Liquid feed rate (ml/min) | 50-90 |
| Gas feed rate (ml/min) | 50-100 |

**Table 2**
Physical properties of three different solvents (303K).

| | bmim[triflate] | emim [$EtSO_4$] | emim[$C_2N_3$] | Ref. |
|---|---|---|---|---|
| Molecular weight (g/mol) | 288.29 | 236.27 | 177.21 | [37] |
| Density ($g/cm^3$) | 1.12 | 1.237 | 1.108 | [38–40] |
| Viscosity (mPa·s) | 100 | 123.5 | 80 | [41] |

The porosity of a hollow fiber ceramic membrane may differ based on the membrane and its intended application. Nonetheless, typically, the porosity of a hollow fiber ceramic membrane can span approximately 30% or higher to 50% [42]. he density ( $\rho$ )and viscosity ( $\mu$ ) of [emim][$EtSO_4$] as a function of temperature [43].

$$\rho\left( \frac{g}{cm^3} \right) = 1.2541 - 5.98\times10^{-4}\left( T(K) - 273.15 \right) \tag{10}$$

$$\mu(mPa.s) = 5.68\times10^{-3}T(K)^{0.5}\exp\left( \frac{945}{T(K)-162} \right) \tag{11}$$

The Henry law solubility constant ( $H_k$ ) of [emim][$EtSO_4$] as a function of temperature at moderate pressure is described by the following correlation [44].

$$H_k\,(Pa) = \exp\left(1.2492 + 0.005949T(K) - 1100/T(K)\right) \tag{12}$$

The distribution factor of $CO_2$ is influenced by the density of the ionic liquid $\rho\left(kg\,m^{-3}\right)$, the ideal gas constant $R\left(8.314\,J\,mol^{-1}K^{-1}\right)$, the temperature $T(K)$, Henry law solubility constant for $CO_2$ in ionic liquid $H_k\,(Pa)$ , and the molecular weight of the ionic liquid ( $M_w$ ) [45].

$$m = \rho RT / M_w H_k \tag{13}$$

Henry's constant, at moderate pressure ( $H_k$ ) states that the solubility of a gas in a liquid is directly proportional to the partial pressure of the gas above the liquid. In other words, as the temperature increases, the solubility of gases in liquids generally decreases. The kinetic theory of gases can explain the relationship between Henry's law of solubility and temperature. According to this theory, as the temperature rises, the kinetic energy of gas molecules increases, leading to more rapid and energetic motion. This increased molecular motion reduces the ability of gas molecules to interact and become trapped within the liquid phase, resulting in lower solubility. Conversely, when the temperature decreases, the kinetic energy of gas molecules decreases, causing them to move more slowly. This slower movement allows gas molecules to interact and dissolve more readily in the liquid, resulting in higher solubility. Overall, Henry's law solubility is inversely affected by temperature, with higher temperatures generally leading to lower solubilities and lower temperatures leading to higher solubilities.

**Table 3**
Physical and chemical preparties used in modeling and simulation.

| Parameters | value | Reference |
|---|---|---|
| $D_{CO_2,g}\left(m^2.s^{-1}\right)$ | $1.55\times10^{-5}$ | [35] |
| $V_{CO_2}\left(cm^3/mol\right)$ | 34 | [46] |
| $D_{CO_2,m}\left(m^2.s^{-1}\right)$ | $D_{CO_2,g}\,(\epsilon/\tau)$ | [47] |
| $D_{CO_2,il}\,(cm^2.s^{-1})$ | $2.66\times10^3\,\mu^{-0.66}v_{CO_2}^{-1.04}$ | [48] |
| Porosity ( $\epsilon$ ) | 0.40 | [49] |
| Tortuosity ( $\tau$ ) | $(2-\epsilon)^2/\epsilon$ | [50] |

The COMSOL Multiphysics version 6.1 software program was employed to develop a model for transporting $CO_2$ through a tube side, dry membrane, and shell side. The model utilized a Cartesian coordinate system to predict the $CO_2$ concentration at various locations within the system. We have employed structured multi-block grids to mesh the system to ensure high accuracy in the calculation and account for the flow field characteristics [51]. The liquid film region, where the flow phenomenon is complex, and the concentration gradient is the largest, is meshed most densely. In contrast, the shell side region experiences a more straightforward flow phenomenon with small

velocity changes and is meshed less densely. The resulting mesh, as shown in Fig. 2, comprises 55,000 elements. This information is shown in Fig. 2, which presumably provides a visual representation of the meshing scheme.

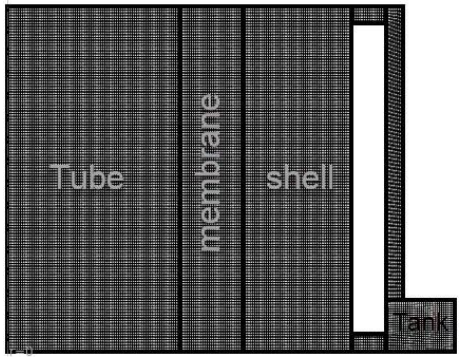


**Fig. 2**. Optimal mesh generation for the four domains (tube, membrane, shell, and ILs tank) of hollow fiber membrane contactor using COMSOL Multiphysics 6.1.

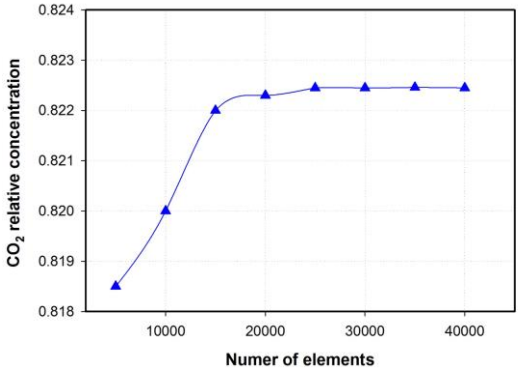


**Fig. 3**. Mesh Refinement convergence graph - mesh elements vs. of the $CO_2$ relative concentration, gas feed rate 50 ml/min, the liquid feed rate is 60 ml/min, and the temperature is 300 K.

Fig. 3 presents the mesh analysis method to simulate and compute the $CO_2$ removal fraction in a hollow fiber membrane contactor. The plot in Fig. 3 shows how varying mesh density (number of elements) affects the mesh convergence and $CO_2$ exit concentration. The concentration of $CO_2$ in the exit stream of a reactor varied with the number of elements in the mesh until it reached a mesh number of around 35,000. Beyond this point, further refinement in the mesh did not significantly change the $CO_2$ concentration in the exit stream.

## 3. Results and discussion

### 3.1. Model validation

Fig. 4 shows the breakthrough curve of the dimensionless exit concentration of $CO_2$ from the tube side, increasing with time until $CO_2$ emerges from the membrane lumen side without being absorbed can be justified by the solvent saturation. As the $CO_2$-containing feed gas passes through the tubular membrane system, the solvent initially exhibits a high absorption capacity, gradually increasing the exit concentration. However, as the solvent becomes saturated, it reaches its maximum capacity to absorb $CO_2$, resulting in a plateau in the breakthrough curve. This is attributed to mass transfer and solubility limitations, where the ability of the ionic liquid solvent to absorb more $CO_2$ declines. The breakthrough profile indicates the need to regenerate the solvent, add fresh solvent, or use an alternative high-absorption capacity solvent [26,53].

Fig. 5 shows the relative concentration of $CO_2$ when the solvent circulation rate is 60 ml/min, and the gas feed rate is 50 ml/min. Initially, there was a discrepancy between the model predictions and experimental data due to system instability and the possible time lag between the membrane module and gas analyzer [54]. However, after 30 minutes, the concentration profile fully developed and there was good agreement between simulation results and experimental data. Initially, for the first 3 min, the system exhibited almost full removal of $CO_2$, almost an efficiency of 100% for the initial recirculation rates of 60 ml/min, and gas feed rates of 50 ml/min. This high efficiency was measured by successfully removing $CO_2$ from the gas side. However, as recirculation continued, the system's efficiency gradually decreased [55].

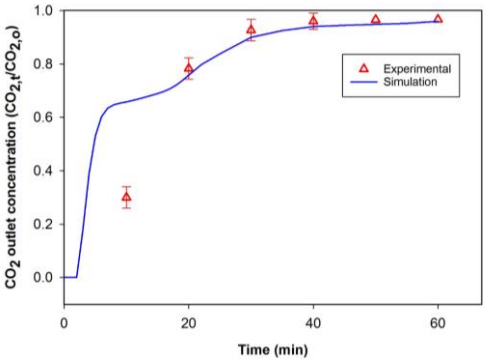


**Fig. 4**. Comparison of current model prediction and experimental data for $CO_2$ absorption [52] with operation time at fixed IL circulation rate (60 ml/min) and gas feed rate (100 ml/min), and 15% $CO_2$ balance is $N_2$.

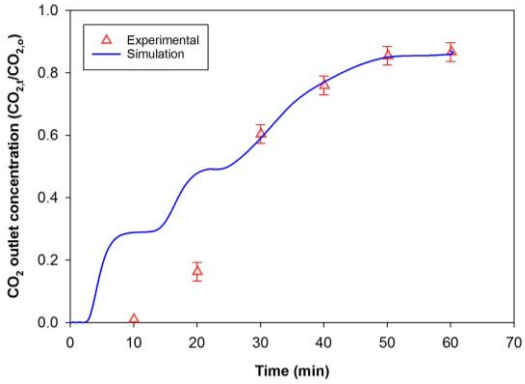


**Fig. 5.** Model validation, $CO_2$ average dimensionless concentration versus time under dry membrane mode, liquid circulation rate is 60 ml/min, and the gas feed rate is 50 ml/min.

### 3.2. Effect of diverse types of ionic liquids

The choice of diverse types of ionic liquids can have a significant effect on $CO_2$ absorption processes. Ionic liquids are a diverse class of compounds with various chemical structures and properties, which can influence their performance as solvents for $CO_2$ absorption. Different ionic liquids can exhibit varying degrees of solubility for $CO_2$. The selectivity of an ionic liquid refers to its ability to preferentially absorb $CO_2$ over other gases present in a gas mixture. Ionic liquids can vary in viscosity, affecting their fluid dynamics and mass transfer properties. Higher viscosities may hinder the mass transfer of $CO_2$ between the gas and liquid phases, leading to slower absorption rates. Overall, the selection of diverse types of ionic liquids allows for the optimization of $CO_2$ absorption processes by tailoring the solubility, selectivity, viscosity, stability, and environmental impact to the specific requirements and objectives of the application. Fig. 6 displays the change in the tube gas dimensionless exit concentration with time for three diverse types of ionic liquids: bmim [Triflate], emim [$EtSO_4$], and emim[$C_2N_2$]. It is observed that, at a fixed time, the exit dimensionless concentration of bmim [Triflate] is greater than that of emim [$EtSO_4$] and emim[$C_2N_2$]. This discrepancy suggests that emim[$C_2N_2$] exhibits a higher potential for absorbing more $CO_2$ than the other two ionic liquids. This finding can be attributed to the lower molecular weight of emim[$C_2N_2$] compared to the other two, which positively influences the distribution factor.

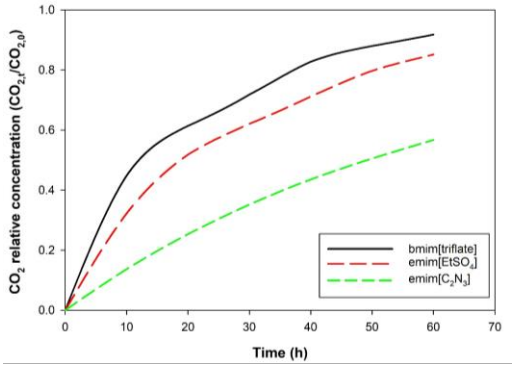


**Fig. 6**. Tube side exit dimensionless concentrations versus time for various ionic liquids. Solvent flow rate 60 ml/min, gas feed rate 50 ml/min.

Upon comparing the three ionic liquids, it becomes apparent that bmim [Triflate] exhibits the highest relative concentration compared to the other two. This signifies the poorer $CO_2$ capture capacity and absorption capability. Conversely, emim[$C_2N_2$] demonstrates a relatively lower exit dimensionless concentration compared to bmim [Triflate], followed by emim [$EtSO_4$]. This suggests that emim[$C_2N_2$] exhibits a stronger $CO_2$ absorption capacity than emim [$EtSO_4$]. The molecular weight of the ionic liquids plays a crucial role in their $CO_2$ absorption capabilities. In this instance, emim[$C_2N_2$] possesses a lower molecular weight than bmim [Triflate] and emim [EtSO4]. This lower molecular weight enhances $CO_2$ solubility and interaction, leading to a higher distribution factor. The distribution factor denotes an ionic liquid's ability to distribute and absorb more $CO_2$ within its structure.

### 3.3. Effect of temperature

Fig. 7 presents the impact of temperature on the relative $CO_2$ concentration in the membrane tube side with operation time. The results revealed that, as the temperature increases the amount of $CO_2$ absorbed drops and accordingly the relative concentration increases. That is attributed to the decrease in the $CO_2$ distribution factor with temperature increases (eq (12)). The distribution factor is directly proportional to the operating temperature and inversely relative to Henry's constant of $CO_2$ at zero pressure in the investigated ionic liquids. It looks that Henry's constant has a dominant influence on the distribution factor as it increases with temperature increases [44]. The $CO_2$ solubility in ILs decreases with temperature increases. The density and viscosity of ILs decrease with temperature increases. The reduced viscosity influences the mass transfer characteristics of the system.

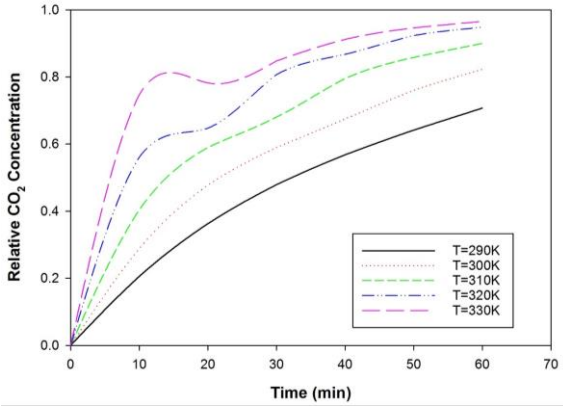


**Fig. 7**. On the tube side, $CO_2$ relative concentrations versus time at various temperatures. Liquid flow rate 60 ml/min, gas feed rate 50 ml/min.

### 3.4. Effect of storage tank size

The size of the storage tank for an ionic liquid can impact the circulation rate in $CO_2$ absorption processes, but it is not a direct or primary factor. The critical role of the storage tank is to provide an adequate supply of ionic liquid for the absorption process rather than directly influencing the circulation rate. The size of the storage tank can indirectly influence the circulation rate by providing a sufficient volume of ionic liquid to maintain the desired flow rate over a specific duration. A larger storage tank may allow for longer continuous operation or accommodate higher circulation rates without frequent refills. Fig. 8 presents the circulation profile of the solvent. It shows the path of the solvent as it enters the upper section of the membrane shell side and exits through the other side into the tank. These specific values enable researchers to assess the system's behavior under controlled conditions and draw meaningful conclusions regarding its functionality and potential improvements. Fig. 8 illustrates the relative outlet concentrations of $CO_2$ in the complete membrane module and the ionic liquid storage tank following 20 minutes of operation. The ionic liquid circulation rate was 60 ml/min, while the gas feed rate was 50 ml/min. The figures show the concentration flux profile.

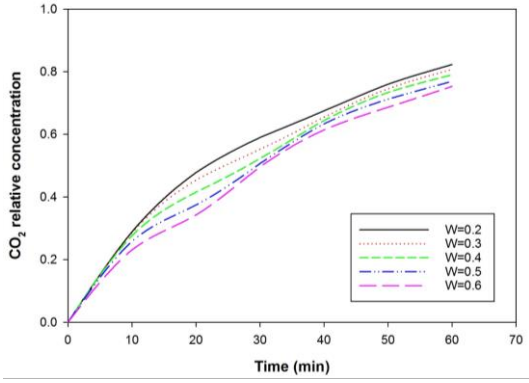


**Fig. 8**. Tube side $CO_2$ relative concentrations versus time at various ionic liquid storage tank sizes. Liquid flow rate 60 ml/min, gas feed rate 50 ml/min, temperature 300K.

### 3.5. Effect of gas feed rate

In the present HFMC configuration, the gas flows in the tube side and the IL flows in the shell side counter-currently. Fig. 9a presents the influence of gas feed rate on the relative $CO_2$ concentration. As the gas feed rate increases, the relative $CO_2$ concentration increases which means the percentage of the removal efficiency decreases. The phenomenon is attributed to decreasing residence time with increasing the gas feed rate. In other words, it decreases gas time spent in direct contact with the liquid solvent [56]. Fig. 9b is the enlargement zone of Fig. 9a for the $CO_2$ absorption before 20 min of operation. Fig. 9b reveals that complete separation was observed initially for a period below approximately 4 minutes of operation. The separation drops sharply between 4 and 10 min and then maintains the reactive concentration between 10 to 20 min. that is attributed to the sufficient available amount of solvent to absorb $CO_2$. The absorption gradually dropped after 20 min. Initially, the high removal efficiency is attributed to fully functional fresh liquid and contactor. The sharp increase in the relative concentration (i.e., drop in the removal efficiency) is attributable to the concentration polarization that may occur when the $CO_2$ concentration near the membrane surface becomes significantly lower than in the bulk of the gas stream. The diffusion resistance created due to this concentration gradient slows the mass transfer of $CO_2$ from the gas to the ionic liquid which leads to a reduction in the $CO_2$ removal efficiency. The removal efficiency stabilization between 10 and 20 min. occurs because the dynamical equilibrium is reached between the concentration polarization effects and the rate of mass transfer, resulting in a relatively constant removal efficiency for a certain period. The continuous drop after 20 min of operation is attributed to the saturation of the ionic liquids and can come into play. To maintain higher and more consistent removal efficiency, solvent regeneration or selecting an ionic liquid with higher $CO_2$ affinity [57–59].

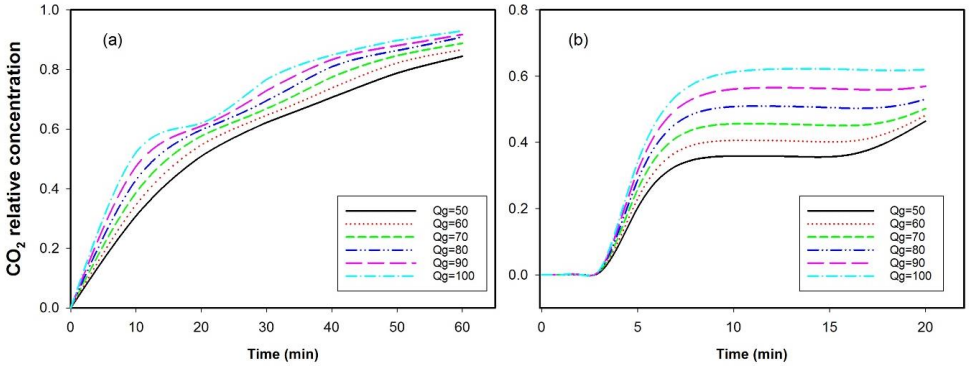


**Fig. 9**. (a)Tube side, $CO_2$ relative concentrations profile versus time at various inlet gas flow rates and constant liquid flow rates (60 ml/min), and fixed temperature (300 K) (b) Enlargement of the zone before 20 min.

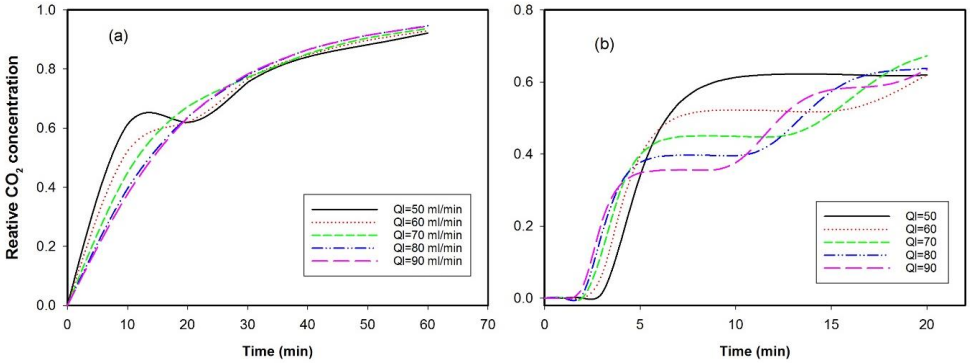


**Fig. 10**. (a) Tube side, $CO_2$ relative concentrations profile versus time at various ionic liquid circulation rates at a constant gas flow rate (100 ml/min) and temperature (300 K) (b) enlargement of the zone within 20 min.

### 3.6. Effect of ionic liquid circulation rate

The effect of ionic liquid circulation rate on the relative $CO_2$ concentration in the tube side of a hollow fiber membrane contactor can vary depending on the specific system and operating conditions (Fig. 10a has been enlarged in Fig. 10b). Increasing the ionic liquid circulation rate on the shell side of the contactor can enhance the mass transfer rate of $CO_2$ across the membrane [52]. This is because a higher flow rate can help maintain a concentration gradient across the membrane, facilitating the transfer of $CO_2$ from the tube side to the shell side. The circulation rate affects the residence time of the ionic liquid in the contactor. A higher circulation rate typically leads to a shorter residence time, meaning the ionic liquid spends less time in contact with the membrane. This can limit the opportunity for $CO_2$ to permeate through the membrane, potentially reducing the $CO_2$ concentration on the tube side [60,61].

### 3.7. Total flux profile

The change in $CO_2$ total flux with time refers to how the total amount of carbon dioxide ($CO_2$) transported or transferred through a system or medium varies over a specific period. Factors such as concentration gradients, diffusion rates, and transport mechanisms can influence $CO_2$ total flux, and the flux can change over time due to alterations in these factors or system conditions [62]. On the other hand, modeling techniques use mathematical equations and computational simulations to predict the behavior of $CO_2$ flux over time. These models consider factors such as concentration gradients, diffusion coefficients, and transport properties to simulate the change in flux. The change in $CO_2$ total flux with time can provide valuable insights into the dynamics of $CO_2$ transport and the efficiency of systems or processes involved in $CO_2$ capture, storage, or transport (Fig. 11). It helps understand how the flux evolves and allows for optimizing and improving $CO_2$ management strategies. With time, more $CO_2$ is absorbed; hence, the $CO_2$ concentration in the ionic liquid circulation region tank increases (Fig. 11). Both Fig. 11 and Fig. 12 work in tandem to depict the concentration flux profile, providing a visual representation of how the $CO_2$ concentrations vary across different system components.

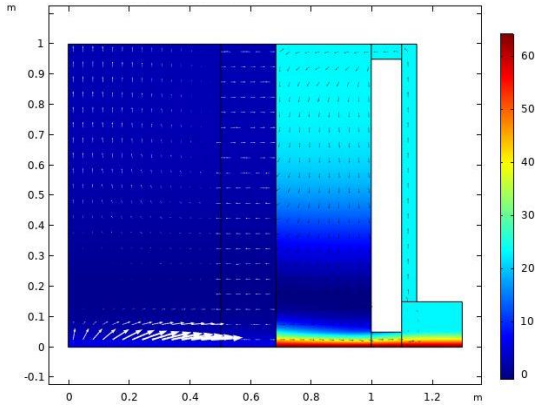

**Fig. 11**. $CO_2$ surface concentrations of $CO_2$ in the complete membrane module and the ionic liquid storage tank following 10 minutes of operation. The ionic liquid circulation rate was 60 ml/min, while the gas feed rate was 50 ml/min.

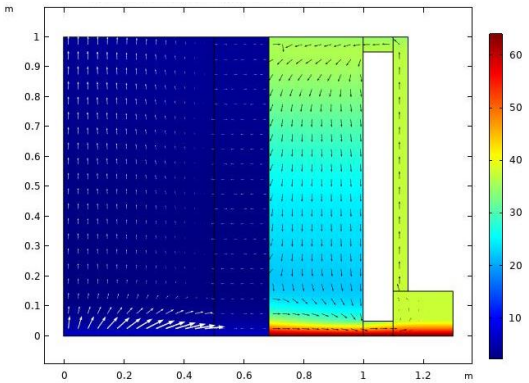

**Fig. 12**. $CO_2$ surface concentrations of $CO_2$ in the complete membrane module and the ionic liquid storage tank following 20 minutes of operation. The ionic liquid circulation rate was 60 ml/min, while the gas feed rate was 50 ml/min.

## 4. Conclusion

This paper presents a novel 2D transient mathematical model that includes the storage tank to simulate $CO_2$ capture using three different ionic liquids (ILs) systems in hollow fiber membrane contactors (HFMCs) while considering the circulation of the IL. The simulation results demonstrate the potential of IL-HFMCs as an efficient approach for $CO_2$ capture, leading to reduced energy consumption and a more favorable environmental footprint. The results indicate that the efficiency of $CO_2$ capture improves as the feed flow rate and $CO_2$ partial pressure increase. Moreover, the transient simulation results suggest that the utilization of IL systems in HFMCs significantly enhances the $CO_2$ capture efficiency compared to other solvents. This article aims to model an approach that significantly contributes to enhancing our understanding of $CO_2$ mass transfer in HFMCs, enabling the improvement of HFMC design and operation for the development of more effective and economically viable $CO_2$ capture technologies. In summary, IL-HFMCs exhibit improved $CO_2$ capture efficiency with higher feed flow rates and $CO_2$ partial pressures, and the modeling presented in this article provides valuable insights into $CO_2$ mass transfer in HFMCs.

## Nomenclature

| | |
|---|---|
| $C_i$ | the molar concentration of component ' $i$ '(mol/m$^3$) |
| $D_i$ | diffusion coefficient (m$^2$/s) |
| $D_{CO_2,g}$ | diffusion coefficient of $CO_2$ in the gas phase (m$^2$/s) |
| $D_{CO_2,il}$ | diffusion coefficient of $CO_2$ in ionic liquid (m$^2$/s) |
| $D_{CO_2,m}$ | diffusion coefficient of $CO_2$ in membrane skin (m$^2$/s) |
| $H_k$ | Henry's law solubility constant for $CO_2$ (Pa) |
| $M_w$ | the molecular weight of the ionic liquid (g/mol) |
| $P$ | the pressure of the fluid (atm) |
| $R$ | Ideal gas constant $\left(8.314\, J\, mol^{-1}K^{-1}\right)$ |
| $R_i$ | the reaction rate (mol/m$^3$.s) |
| $r$ | variable radius (m) |
| $r_1$ | inner tube radius (m) |
| $r_2$ | outer tube radius (m) |
| $T$ | the temperature (K) |
| $V_{av}$ | average velocity (m/s) |
| $V_{CO_2}$ | $CO_2$ molar volume (34 cm$^3$/mol) |
| $V_z$ | the axial velocity along the membrane module length (m/s) |

**Greek symbols**

| | |
|---|---|
| $\epsilon$ | membrane porosity |
| $\tau$ | tortuosity |
| $\rho$ | density of the fluid (kg/m$^3$) |
| $\mu$ | fluid's dynamic viscosity (Pa.s) |

## Acknowledgment

The author would like to acknowledge UAE University for financial support (UPAR grant number: 31N374).

## Data availability

No data was used for the research described in the article.

## Funding

This work was financially supported by the UAEU research office

## CRedit authorship contribution statement

*N. Ghasem*: Conceptualization; Data curation; Formal analysis; Funding acquisition; Investigation; Methodology; Project administration; Resources; Software; Supervision; Validation; Visualization; Writing – original draft; Writing – review & editing.

## Declaration of Competing Interest

The author declares that he has no known competing financial interests or personal relationships that could have appeared to influence the work reported in this paper.

## References

[1] M. Pasichnyk, P. Stanovsky, P. Polezhaev, B. Zach, M. Šyc, M. Bobák, J.C. Jansen, M. Přibyl, J.E. Bara, K. Friess, J. Havlica, D.L. Gin, R.D. Noble, P. Izák, Membrane technology for challenging separations: Removal of CO2, SO2 and NOx from flue and waste gases, Sep. Purif. Technol. 323 (2023). https://doi.org/10.1016/j.seppur.2023.124436.

[2] M.W. Jones, G.P. Peters, T. Gasser, R.M. Andrew, C. Schwingshackl, J. Gütschow, R.A. Houghton, P. Friedlingstein, J. Pongratz, C. Le Quéré, National contributions to climate change due to historical emissions of carbon dioxide, methane, and nitrous oxide since 1850, Sci. Data. 10 (2023) 155. https://doi.org/10.1038/s41597-023-02041-1.

[3] N. Ghasem, CO2 removal from natural gas, in: Adv. Carbon Capture, Elsevier, 2020: pp. 479–501. https://doi.org/10.1016/B978-0-12-819657-1.00021-9.

[4] N. Ghasem, Chemical absorption of CO2 enhanced by nanoparticles using a membrane contactor: Modeling and simulation, Membranes (Basel). 9 (2019). https://doi.org/10.3390/membranes9110150.

[5] Y. Xu, K. Goh, R. Wang, T.-H. Bae, A review on polymer-based membranes for gas-liquid membrane contacting processes: Current challenges and future direction, Sep. Purif. Technol. 229 (2019) 115791. https://doi.org/10.1016/j.seppur.2019.115791.

[6] A. Marjani, A.T. Nakhjiri, M. Pishnamazi, S. Shirazian, Evaluation of potassium glycinate, potassium lysinate, potassium sarcosinate and potassium threonate solutions in CO2 capture using membranes, Arab. J. Chem. 14 (2021) 102979. https://doi.org/10.1016/j.arabjc.2020.102979.

[7] Y. Cao, A. Taghvaie Nakhjiri, M. Ghadiri, CFD investigation of CO2 separation from anesthesia gaseous stream applying novel cholinium lysinate amino acid-based ionic liquid inside the gas-liquid membrane contactor, Eur. Phys. J. Plus. 137 (2022) 1044. https://doi.org/10.1140/epjp/s13360-022-03261-x.

[8] N. Cihan, O.Y. Orhan, H.Y. Ersan, Effect of non-aqueous solvents on kinetics of carbon dioxide absorption by tBu3P/B (C6F5) 3 frustrated Lewis pairs, Sep. Purif. Technol. 258 (2021) 118058. https://doi.org/10.1016/j.seppur.2020.118058.

[9] Z. Rezaeiyan, S. Bagheri, M.A. Sedghamiz, M.R. Rahimpour, Polarity-changing solvents for CO2 capture, in: Green Sustain. Process Chem. Environ. Eng. Sci., Elsevier, 2022: pp. 21–37. https://doi.org/10.1016/B978-0-12-819850-6.00003-6.

[10] A. Hedayati, F. Feyzi, Three-component 1, 1, 3, 3-tetramethylguanidine based CO2-binding organic liquids: Statistical solvent design and thermodynamic modeling of CO2 solubility by LJ-Global TPT2 EoS, Fluid Phase Equilib. 565 (2023) 113645. https://doi.org/10.1016/j.fluid.2022.113645.

[11] A. Hedayati, F. Feyzi, CO2-binding organic liquids for high-pressure CO2 absorption: Statistical mixture design approach and thermodynamic modeling of CO2 solubility using LJ-Global TPT2 EoS, J. Mol. Liq. 337 (2021) 116396. https://doi.org/10.1016/j.molliq.2021.116396.

[12] A. Hedayati, F. Feyzi, Towards water-insensitive CO2-binding organic liquids for CO2 absorption: Effect of amines as promoter, J. Mol. Liq. 306 (2020) 112938. https://doi.org/10.1016/j.molliq.2020.112938.

[13] D. Li, C. Li, Efficient and Reversible Capture of CO2 in CO2-Binding Organic Liquids Formed by 1, 1, 3, 3-Tetramethylguanidine and Glycerol Derivatives, ACS Sustain. Chem. Eng. (2023). https://doi.org/10.1021/acssuschemeng.2c05109.

[14] D.J. Heldebrant, P.K. Koech, J.E. Rainbolt, F. Zheng, T. Smurthwaite, C.J. Freeman, M. Oss, I. Leito, Performance of single-component CO2-binding organic liquids (CO2BOLs) for post-combustion CO2 capture, Chem. Eng. J. 171 (2011) 794–800. https://doi.org/10.1016/j.cej.2011.02.012.

[15] Y. Park, K.-Y.A. Lin, A.-H.A. Park, C. Petit, Recent advances in anhydrous solvents for CO2 capture: ionic liquids, switchable solvents, and nanoparticle organic hybrid materials, Front. Energy Res. 3 (2015) 42. https://doi.org/10.3389/fenrg.2015.00042.

[16] N. Ghasem, M. Al-Marzouqi, Modeling and experimental study of carbon dioxide absorption in a flat sheet membrane contactor, J. Membr. Sci. Res. 3 (2017). https://doi.org/10.22079/jmsr.2016.20226.
[17] P. Zare, P. Keshavarz, D. Mowla, Membrane absorption coupling process for CO2 capture: application of water-based ZnO, TiO2, and multi-walled carbon nanotube nanofluids, Energy & Fuels. 33 (2019) 1392–1403. https://doi.org/10.1021/acs.energyfuels.8b03972.
[18] J.M. Vadillo, L. Gomez-Coma, A. Garea, A. Irabien, Hollow fiber membrane contactors in CO2 desorption: A review, Energy & Fuels. 35 (2020) 111–136. https://doi.org/10.1021/acs.energyfuels.0c03427.
[19] M. Rasaie, A. Elhambakhsh, M. Eskandari, P. Keshavarz, D. Mowla, Highly selective physical/chemical CO2 separation by functionalized Fe3O4 nanoparticles in hollow fiber membrane contactors: experimental and modeling approaches, Energy & Fuels. 36 (2022) 4456–4469. https://doi.org/10.1021/acs.energyfuels.2c00219.
[20] M. Mesbah, M. Momeni, E. Soroush, S. Shahsavari, S.A. Galledari, Theoretical study of CO2 separation from CO2/CH4 gaseous mixture using 2-methylpiperazine-promoted potassium carbonate through hollow fiber membrane contactor, J. Environ. Chem. Eng. 7 (2019) 102781. https://doi.org/10.1016/j.jece.2018.11.026.
[21] K.M. Diederichsen, T.A. Hatton, Nondimensional Analysis of a Hollow Fiber Membrane Contactor for Direct Air Capture, Ind. Eng. Chem. Res. 61 (2022) 11964–11976. https://doi.org/10.1021/acs.iecr.2c02206.
[22] Y. Cao, A. Khan, A.T. Nakhjiri, A.B. Albadarin, T.A. Kurniawan, M. Rezakazemi, Recent advancements in molecular separation of gases using microporous membrane systems: A comprehensive review on the applied liquid absorbents, J. Mol. Liq. 337 (2021) 116439. https://doi.org/10.1016/j.molliq.2021.116439.
[23] N. Ghasem, Modeling and Simulation of CO2 Absorption Enhancement in Hollow-Fiber Membrane Contactors using CNT–Water-Based Nanofluids, J. Membr. Sci. Res. 5 (2019) 295–302. https://doi.org/10.22079/jmsr.2019.100177.1239.
[24] M. Aghaie, N. Rezaei, S. Zendehboudi, A systematic review on CO2 capture with ionic liquids: Current status and future prospects, Renew. Sustain. Energy Rev. 96 (2018) 502–525. https://doi.org/10.1016/j.rser.2018.07.004.
[25] M. Darabi, H. Pahlavanzadeh, Mathematical modeling of CO2 membrane absorption system using ionic liquid solutions, Chem. Eng. Process. - Process Intensif. 147 (2020) 107743. https://doi.org/10.1016/j.cep.2019.107743.
[26] Y. Qu, Y. Zhao, D. Li, J. Sun, Task-specific ionic liquids for carbon dioxide absorption and conversion into value-added products, Curr. Opin. Green Sustain. Chem. 34 (2022) 100599. https://doi.org/10.1016/j.cogsc.2022.100599.
[27] A. Taghvaie Nakhjiri, M. Davidson, Modeling and Simulation of Natural Convection Heat transfer Process In porous and non-porous media, Appl. Res. J. 2 (2016) 199–204.
[28] H.-Y. Zhang, R. Wang, D. Liang, J.-H. Tay, Modeling and experimental study of CO2 absorption in a hollow fiber membrane contactor, J. Membr. Sci. - J Membr. SCI. 279 (2006) 301–310. https://doi.org/10.1016/j.memsci.2005.12.017.
[29] N. Ghasem, Efficient CO2 absorption through wet and falling film membrane contactors: insights from modeling and simulation, Sci. Rep. 13 (2023) 10994. https://doi.org/10.1038/s41598-023-38249-9.
[30] E.N. Fuller, P.D. Schettler, J.C. Giddings, NEW METHOD FOR PREDICTION OF BINARY GAS-PHASE DIFFUSION COEFFICIENTS, Ind. Eng. Chem. 58 (1966) 18–27. https://doi.org/10.1021/ie50677a007.
[31] R.B. Bird, W.E. Stewai, E.N. Lightfoot, Phenomena Second Edition, (n.d.).
[32] J.C. Slattery, Advanced transport phenomena, Cambridge University Press, 1999.
[33] N. Ghasem, CFD simulation of CO2 absorption by water-based TiO2 nanoparticles in a high pressure stirred vessel, Sci. Rep. 11 (2021) 1984. https://doi.org/10.1038/s41598-021-81406-1.
[34] N. Ghasem, Modeling and Simulation of the Simultaneous Absorption/Stripping of CO2 with Potassium Glycinate Solution in Membrane Contactor, Membranes (Basel). 10 (2020). https://doi.org/10.3390/membranes10040072.
[35] Q. Sohaib, L. Gomez-Coma, J. Albo, S. Druon-Bocquet, A. Irabien, J. Sanchez Marcano, CO2 Capture in a Hollow Fiber Membrane Contactor Coupled with Ionic Liquid: Influence of Membrane Wetting and Process Parameters, Sep. Purif. Technol. 233 (2019) 115986. https://doi.org/10.1016/j.seppur.2019.115986.
[36] W. Qi, K. Fu, X. Chen, M. Qiu, Y. Fan, Falling liquid-film on hydrophilic porous ceramic membrane for boosting CO2 absorption, Sep. Purif. Technol. 303 (2022) 122238. https://doi.org/10.1016/j.seppur.2022.122238.
[37] J.-H. Yim, S.-J. Ha, J.S. Lim, Measurement and correlation of CO2 solubility in 1-ethyl-3-methylimidazolium ([EMIM]) cation-based ionic liquids:[EMIM][Ac],[EMIM][Cl], and [EMIM][MeSO4], J. Chem. Eng. Data. 63 (2018) 508–518. https://doi.org/10.1021/acs.jced.7b00532.
[38] J. Safarov, A. Guluzade, Density and Molar Volumes of 1-Butyl-3-methylimidazolium trifluoromethanesulfonate and Methanol Mixtures at Ambient and Saturated Pressures, Int. J. Thermophys. 43 (2022) 104. https://doi.org/10.1007/s10765-022-03014-z.
[39] R.A. Mantz, P. Trulove, Viscosity and density of ionic liquids, Ion. Liq. Synth. 2 (2003) 56–68.
[40] H. Schmidt, M. Stephan, J. Safarov, I. Kul, J. Nocke, I.M. Abdulagatov, E. Hassel, Experimental study of the density and viscosity of 1-ethyl-3-methylimidazolium ethyl sulfate, J. Chem. Thermodyn. 47 (2012) 68–75. https://doi.org/10.1016/j.jct.2011.09.027.
[41] K. Paduszyński, U. Domańska, Viscosity of Ionic Liquids: An Extensive Database and a New Group Contribution Model Based on a Feed-Forward Artificial Neural Network, J. Chem. Inf. Model. 54 (2014) 1311–1324. https://doi.org/10.1021/ci500206u.
[42] Y. Li, Y. Ma, Y. Li, S. Li, Processing and microstructure-permeation properties of silica bonded silicon carbide ceramic membrane, J. Eur. Ceram. Soc. 41 (2021) 7525–7532. https://doi.org/10.1016/j.jeurceramsoc.2021.08.015.
[43] J. Jacquemin, P. Husson, A.A.H. Padua, V. Majer, Density and viscosity of several pure and water-saturated ionic liquids, Green Chem. 8 (2006) 172–180. https://doi.org/10.1039/B513231B.
[44] A.N. Soriano, B.T. Doma, M.-H. Li, Carbon dioxide solubility in some ionic liquids at moderate pressures, J. Taiwan Inst. Chem. Eng. 40 (2009) 387–393. https://doi.org/10.1016/j.jtice.2008.12.002.
[45] Q. Sohaib, M.A. Kazemi, C. Charmette, J. Cartier, M. Younas, A. Azarafza, M. Rezakazemi, J. Sanchez-Marcano, CO2 solubility and diffusivity in 1-ethyl-3-methylimidazolium cation-based ionic liquids; isochoric pressure drop approach, Fluid Phase Equilib. 563 (2022) 113581. https://doi.org/10.1016/j.fluid.2022.113581.
[46] W. Hayduk, S.C. Cheng, Review of relation between diffusivity and solvent viscosity in dilute liquid solutions, Chem. Eng. Sci. 26 (1971) 635–646. https://doi.org/10.1016/0009-2509 (71)86007-4.
[47] A.T. Nakhjiri, A. Heydarinasab, O. Bakhtiari, T. Mohammadi, Modeling and simulation of CO2 separation from CO2/CH4 gaseous mixture using potassium glycinate, potassium argininate and sodium hydroxide liquid absorbents in the hollow fiber membrane contactor, J. Environ. Chem. Eng. 6 (2018) 1500–1511. https://doi.org/10.1016/j.jece.2018.01.068.
[48] Y. Hou, R.E. Baltus, Experimental Measurement of the Solubility and Diffusivity of CO2 in Room-Temperature Ionic Liquids Using a Transient Thin-Liquid-Film Method, Ind. Eng. Chem. Res. 46 (2007) 8166–8175. https://doi.org/10.1021/ie070501u.
[49] E. Magnone, H.J. Lee, M.C. Shin, J.H. Park, A performance comparison study of five single and sixteen blended amine absorbents for CO2 capture using ceramic hollow fiber membrane contactors, J. Ind. Eng. Chem. 100 (2021) 174–185. https://doi.org/10.1016/j.jiec.2021.05.025.
[50] S.B. Iversen, V.K. Bhatia, K. Dam-Johansen, G. Jonsson, Characterization of microporous membranes for use in membrane contactors, J. Memb. Sci. 130 (1997) 205–217. https://doi.org/10.1016/S0376-7388 (97)00026-4.
[51] M. Ozkutlu, O.Y. Orhan, H.Y. Ersan, E. Alper, Kinetics of CO2 capture by ionic liquid—CO2 binding organic liquid dual systems, Chem. Eng. Process. Process Intensif. 101 (2016) 50–55. https://doi.org/10.1016/j.cep.2015.12.011.
[52] S. Qazi, L. Gómez-Coma, J. Albo, S. Druon-Bocquet, A. Irabien, J. Sanchez-Marcano, CO2 capture in a hollow fiber membrane contactor coupled with ionic liquid: Influence of membrane wetting and process parameters, Sep. Purif. Technol. 233 (2020) 115986. https://doi.org/10.1016/j.seppur.2019.115986.
[53] E. Kayahan, U. Di Caprio, A. Van den Bogaert, M.N. Khan, M. Bulut, L. Braeken, T. Van Gerven, M.E. Leblebici, A new look to the old solvent: Mass transfer performance and mechanism of CO2 absorption into pure monoethanolamine in a spray column, Chem. Eng. Process. - Process Intensif. 184 (2023) 109285. https://doi.org/10.1016/j.cep.2023.109285.
[54] H. Wu, N. Al-Qasas, B. Kruczek, J. Thibault, Simulation of Time-Lag Permeation Experiments Using Finite Differences, J. Fluid Flow, Heat Mass Transf. 2 (2015). https://doi.org/10.11159/jffhmt.2015.003.
[55] Z. Dai, L. Deng, Membrane absorption using ionic liquid for pre-combustion CO2 capture at elevated pressure and temperature, Int. J. Greenh. Gas Control. 54 (2016) 59–69. https://doi.org/10.1016/j.ijggc.2016.09.001.
[56] A. Imtiaz, M.H.D. Othman, A. Jilani, I.U. Khan, R. Kamaludin, M. Ayub, O. Samuel, T.A. Kurniawan, N. Hashim, M.H. Puteh, A critical review in

recent progress of hollow fiber membrane contactors for efficient CO2 separations, Chemosphere. 325 (2023) 138300. https://doi.org/10.1016/j.chemosphere.2023.138300.

[57] R. Nasir, D.F. Mohshim, H.A. Mannan, D. Qadir, H. Mukhtar, K. Maqsood, A. Ali, B. Maulianda, A. Abdulrahman, A. Bin Mahfouz, A perspective on ionic liquid-based membranes for CO2 separation, Chem. Pap. 75 (2021) 839–852. https://doi.org/10.1007/s11696-020-01384-y.

[58] H. Gao, L. Bai, J. Han, B. Yang, S. Zhang, X. Zhang, Functionalized ionic liquid membranes for CO2 separation, Chem. Commun. 54 (2018) 12671–12685. https://doi.org/10.1039/C8CC07348A.

[59] S. Zeng, X. Zhang, L. Bai, X. Zhang, H. Wang, J. Wang, D. Bao, M. Li, X. Liu, S. Zhang, Ionic-Liquid-Based CO2 Capture Systems: Structure, Interaction and Process, Chem. Rev. 117 (2017) 9625–9673. https://doi.org/10.1021/acs.chemrev.7b00072.

[60] S. Kim, C.A. Scholes, D.E. Heath, S.E. Kentish, Gas-liquid membrane contactors for carbon dioxide separation: A review, Chem. Eng. J. 411 (2021) 128468. https://doi.org/10.1016/j.cej.2021.128468.

[61] K. Simons, K. Nijmeijer, M. Wessling,Gas–liquid membrane contactors for CO2 removal, J. Memb. Sci. 340 (2009) 214–220. https://doi.org/10.1016/j.memsci.2009.05.035.

[62] M. Li, Z. Zhu, M. Zhou, X. Jie, L. Wang, G. Kang, Y. Cao, Removal of CO2 from biogas by membrane contactor using PTFE hollow fibers with smaller diameter, J. Memb. Sci. 627 (2021) 119232. https://doi.org/10.1016/j.memsci.2021.119232.